Generation of the windowed multipole resonance data using Vector Fitting technique

Citation: Liu, Shichang et al. "Generation of the windowed multipole resonance data using Vector Fitting technique." Annals of Nuclear Energy 112 (February 2018): 30-41. © 2017 Elsevier Ltd

As Published: http://dx.doi.org/10.1016/j.anucene.2017.09.042

Publisher: Elsevier BV

Persistent URL: https://hdl.handle.net/1721.1/125299

Version: Author's final manuscript: final author's manuscript post peer review, without publisher's formatting or copy editing

Generation of the Windowed Multipole Resonance Data Using Vector Fitting Technique

Shichang Liu[a], Xingjie Peng[b,c], Colin Josey[b], Jingang Liang[b], Benoit Forget[b*], Kord Smith[b], Kan Wang[a]

[a] *Department of Engineering Physics, Tsinghua University, Beijing 100084, China*

[b] *Department of Nuclear Science and Engineering, Massachusetts Institute of Technology, Cambridge, Massachusetts, 02139, USA*

[c] *Science and Technology on Reactor System Design Technology Laboratory, Nuclear Power Institute of China, Chengdu, Sichuan 610000, China*

Abstract

The multipole representation provides an analytical way of Doppler broadening cross sections for neutron interactions and relies on a partial fraction decomposition that represents R-matrix resonance parameters by poles and residues. The windowed multipole method selectively broadens impactful poles and approximates the rest to increase the efficiency of the process. However, this process requires knowledge of the resonance parameters and certain limitations occur when additional channels are opened in the defined resolved resonance region such that only 2/3 of the ENDF/B-VII.1 nuclides can be processed. Some important nuclides needed in reactor applications such as Oxygen-16 and Hydrogen-1 are directly represented in pointwise form in the evaluation nuclear data library hindering the practicality of this approach. This paper presents a new fitting method for nuclear point-wise cross sections data that yields a pole and residue form analogous to the multipole representation. The Vector Fitting technique which originates from the field of signal processing was applied to the fitting of point-wise cross sections. Poles and residues from Vector Fitting were generated for Oxygen-16, Hydrogen-1, Boron-10 and Boron-11 and processed in the windowed multipole format. These new libraries were tested by direct comparison of the microscopic cross sections before and after Doppler Broadening, and by integral comparisons using a typical PWR pin cell from the BEAVRS benchmark. Results indicate that the new libraries are equivalent to the point-wise representation with the added benefit of allowing on-the-fly Doppler broadening without the need for temperature interpolation. Runtimes are approximately ~28% slower using the multipole representation on this example problem compared to a single temperature ACE file.

Key words: Monte Carlo, Multipole, Doppler broadening, Vector Fitting, OpenMC

* Corresponding author.
E-mail addresses: liu-sc13@mails.tsinghua.edu.cn (S. Liu), bforget@mit.edu (B. Forget)

1. Introduction

With increasing computing power, Monte Carlo methods have become more widely used for temperature dependent coupled simulations (Herman, 2014; Wang, 2017). To enable these simulations, temperature dependent microscopic cross sections are needed without substantially impacting the simulation runtime or significantly increasing the memory requirements. Many on-the-fly Doppler broadening methods have been proposed over the years that are either based on direct integration of the point-wise data by various means (Cullen and Weisbin, 1976; Romano, 2015), high order temperature fits (Yesilyurt et al., 2012), stochastic sampling (Becker et al. 2009) or rejection based sampling (Viitanen and Leppanen, 2012). These methods have been applied with varying levels of success, often making tradeoffs between memory and efficiency.

Recently a new approach was proposed that relies on the partial fraction decomposition of the fundamental R-matrix representation of the cross section. This transformation replaces traditional resonance parameters by poles and residues with the added advantage of enabling analytical Doppler broadening using this new resonance representation. The windowed multipole method gets its efficiency by Doppler broadening only local resonances and neglecting temperature effects caused by far away resonances (Forget, 2014). Several optimizations have been proposed in the determination of optimal parameters for the windowing process and fitting of the non-Doppler broadened resonances (Josey, 2014; Josey, 2015). However, this methodology has a major shortcoming in that it can only Doppler broaden nuclear data using given resonance parameters. Many light nuclides, for example, are provided in ENDF/B-VII.1 directly in point-wise data either due to shortcomings in the common processing codes or the evaluation format. To make the windowed multipole method practical, an alternate Doppler broadening approach would be needed unless the point-wise data could also be represented in the pole and residue form.

In this article, a new method based on Vector Fitting technique is proposed to compute poles and residues from the point-wise cross sections data, which can then be processed in the windowed multipole form. This new approach can potentially address the major shortcoming of the windowed multipole method and represent all needed nuclides in the same format. Section 2 introduces the background of the multipole representation and windowed multipole method. Section 3 presents the difficulties of pole fitting using rational function and traditional least square methods, which are resolved by the Vector Fitting technique. Section 4 introduces the procedure to generate a window multipole library from point-wise data. Section 5 provides microscopic comparisons of the generated cross sections of Oxygen-16, Hydrogen-1, Boron-10 and Boron-11. The accuracy and performance of the generated windowed multipole libraries were then tested on a typical PWR fuel pin. Finally, the conclusions are presented in Section 6.

2. Multipole representation and windowed multipole method

2.1. Multipole representation and Doppler broadening

The foundation of the multipole representation is the R-matrix theory, which in nuclear engineering is commonly simplified to the Reich–Moore formalism and the Multi-Level Breit–Wigner (MLBW) formalism (Hwang, 1987). Based on the Reich–Moore formalism, the neutron cross section of reaction x and total cross section at 0 K can be expressed as rational functions with poles and residues as written here:

$$\sigma_x(E) = \frac{1}{E}\sum_{l,J}\sum_{\lambda=1}^{N}\sum_{j=1}^{2(l+1)} \mathrm{Re}\left[\frac{-ir_{x\lambda}^{(j)}}{p_\lambda^{(j)*} - \sqrt{E}}\right] \tag{1}$$

$$\sigma_t(E) = \sigma_p(E) + \frac{1}{E}\sum_{l,J}\sum_{\lambda=1}^{N}\sum_{j=1}^{2(l+1)} \mathrm{Re}\left[\exp(-i2\phi_l)\frac{-ir_{t\lambda}^{(j)}}{p_\lambda^{(j)*} - \sqrt{E}}\right] \tag{2}$$

where the potential cross section is

$$\sigma_p(E) = \sum_{l,J} 4\pi\lambda^2 g_J \sin^2\phi_l \tag{3}$$

$p_\lambda^{(j)}$, $r_{x\lambda}^{(j)}$ and $r_{t\lambda}^{(j)}$ are the pole, residue of reaction x, residue of total cross section associated to resonance λ and pole j. Each reaction type will have a different residue but the poles remain unchanged for a given isotope. In the previous expression, $p_\lambda^{(j)*}$ is the complex conjugate of the pole, N is the number of resonances, the summation from 1 to $2(l+1)$ represents the number of poles for each resonance where l represents the angular momentum of the channel and J represents the channel spin. The spin statistical factor and phase shift parameters in Equation 3 are denoted by g_J and ϕ_l, respectively.

From Equation 1 & 2, the cross sections can be calculated by summing over l, J, N and number of poles for each resonance $(1 \sim 2(l+1))$. These analytical representations can be directly Doppler broadened using the Solbrig kernel (Solbrig, 1961), without any reconstruction to point-wise form. The Doppler broadened cross sections are given by

$$\sigma_x(E,\xi) = \frac{1}{E}\sum_{l,J}\sum_{\lambda=1}^{N}\sum_{j=1}^{2(l+1)} \frac{\mathrm{Re}\left[r_x\sqrt{\pi}W(z_0) - \frac{-ir_x}{\sqrt{\pi}}C\left(\frac{p_\lambda^{(j)*}}{\sqrt{\xi}}, \frac{\sqrt{E}}{2\sqrt{\xi}}\right)\right]}{2\sqrt{\xi}} \tag{4}$$

$$\sigma_t(E,\xi)=\sigma_p(E)+\frac{1}{E}\sum_{l,J}\sum_{\lambda=1}^{N}\sum_{j=1}^{2(l+1)}\frac{\mathrm{Re}\left\{\exp(-i2\phi_l)\left[r_x\sqrt{\pi}W(z_0)-\frac{-ir_t}{\sqrt{\pi}}C\left(\frac{p_\lambda^{(j)*}}{\sqrt{\xi}},\frac{\sqrt{E}}{2\sqrt{\xi}}\right)\right]\right\}}{2\sqrt{\xi}} \quad (5)$$

$$W(z_0)=\exp(-z_0{}^2)erfc(-iz_0) \quad (6)$$

where $\xi=\frac{kT}{4A}$ and $z_0=\frac{\sqrt{E}-p_\lambda^{(j)*}}{2\sqrt{\xi}}$. The Faddeeva function is denoted by $W(z_0)$, with complex argument z_0. The C term in Equation 5 is negligible except at very low energies as noted by Hwang (1987). The cross sections are related to temperature of the medium T via ξ. As different reactions share the same poles and same z_0, the Faddeeva function of each pole can be calculated once and applied to all the reactions.

2.2. Windowed multipole (WMP) method

The most computationally expensive part in Equation 4 & 5 is the Faddeeva function, which should be evaluated for each and every pole. Some important nuclides such as ^{235}U and ^{238}U have thousands of poles once converted from Reich–Moore formalism making the formalism impractical for direct simulation. The windowed multipole method was proposed to improve the efficiency.

From Equation 1 & 2, it can be found that for a given energy point E, the poles p_λ which are close to E have significant contributions to the cross section directly impacted by temperature, while poles far from E have smooth tails that are inherently temperature independent. These smooth contributions can be curve-fitted by low-order polynomials. The concept of inner and outer window has been proposed to identify the poles that should be Doppler broadened, as shown in Fig. 1~~Fig. 1~~.

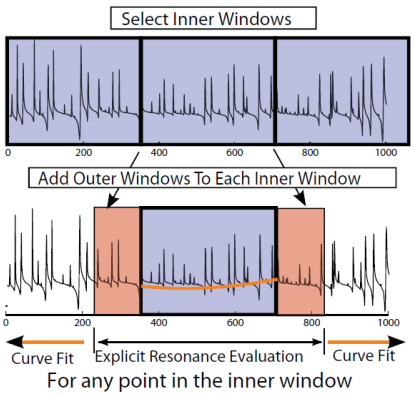

Fig. 1 Concept of inner and outer window (Josey, 2016)

The energy range of a nuclide is divided into inner windows of equal momentum space, which can be considered as domains of definition for a piecewise function. The cross section at energy E located in a given inner window can be represented by the summation of the contributions from the Doppler broadened poles within the outer window and the contribution of the curve fit. Equation 7 presents the form of the polynomials used in the fitting process.

$$\sigma_{CF}(E) = \sum_{i=0}^{N} a_i \left(\sqrt{E}\right)^{i-2} \tag{7}$$

In this way, the cross section can be calculated by only evaluating the Faddeeva functions of poles in the outer window at temperature T. Doppler broadening of the polynomials was also added to further improve efficiency (Josey, 2016).

3. Rational function fitting and Vector Fitting technique

In the ENDF/B-VII.1 library, the resonance parameters used to convert to multipole formalism are not given for all nuclides which are instead provided in point-wise format. Some of these nuclides are important in reactor applications such as Oxygen-16, Hydrogen-1 and the Boron isotopes. The point-wise data are given in pairs of $(E_i, \sigma(E_i))$ which can be ~~linearly~~ interpolated linearly or log-log. To facilitate Doppler broadening as performed in the windowed multipole approach, this paper explores a fitting process that will transform the point-wise data in the same format.

3.1. Least square method

From Equation 1, $\sqrt{E}$ can be treated as the variable $u=\sqrt{E}$, and Equation 1 can be written to

$$\sigma_x(u)*u^2=\sum_{l,J}\sum_{\lambda=1}^{N}\sum_{j=1}^{2(l+1)}\mathrm{Re}\left[\frac{-ir_{x\lambda}^{(j)}}{p_\lambda^{(j)*}-u}\right] \tag{8}$$

As the point-wise data $\left(E_i,\sigma(E_i)\right)$ are given, $y(u)=\sigma_x(u)*u^2$ can be evaluated. Equation 8 can be further written as a rational function, i.e. a ratio of two polynomials.

$$y(u)=\frac{a_0+a_1u+a_2u^2+\cdots+a_{N-1}u^{N-1}}{b_0+b_1u+b_2u^2+\cdots+b_Nu^N} \tag{9}$$

Equation 9 is nonlinear in terms of the unknown coefficients but can be rewritten as a linear problem of the type $Ax=b$ by multiplying both sides with the denominator. Here, the unknowns of vector x include the coefficients $a_0,a_1,a_2,a_{N-1},b_0,b_1,b_2,\cdots b_N$ in Equation 9, and the given point-wise data $\left(E_i,\sigma(E_i)\right)$ which can be changed to $\left(y,u\right)$ will contribute to the matrix A and vector b. Since the number of point-wise data is most likely larger than the number of unknowns, the problem is overdetermined and can be solved using a least squares approach. However, the resulting system of equations is badly scaled and conditioned as the columns in A are multiplied with different powers of u.

3.2. Vector Fitting technique

The Vector Fitting (VF) technique has been widely used in the power systems and microwave engineering communities (Gustavsen, 1999). The VF technique uses partial fractions instead of polynomials to overcome the ill-conditioned nature of the least square method.

Equation 9 can be represented by rational function as shown in Equation 10.

$$f(s)=\sum_{n=1}^{N}\frac{c_n}{s-a_n}+d+e\cdot s \tag{10}$$

In the VF technique, the residues c_n and poles a_n are either real quantities or appear as complex conjugate pairs. For the cross section described by Equation 8, d and e are simply zero. VF solves Equation 10 sequentially in two steps, both times assuming known poles.

The first step is called “pole identification”, which introduces an unknown rational function $h(s)$

$$h(s) = \sum_{n=1}^{N} \frac{\tilde{c}_n}{s - \tilde{a}_n} + 1 \tag{11}$$

where $\{\tilde{a}_n\}$ is a set of initial guessed poles. Multiplying $f(s)$ with $h(s)$ leads to a linear least square problem.

$$h(s) f(s) = p(s) \tag{12}$$

where

$$p(s) = \sum_{n=1}^{N} \frac{c_n}{s - \tilde{a}_n} + d + e \cdot s \tag{13}$$

From Equation 12, it can be found that the poles of $f(s)$ are the zeros of $h(s)$ details of which can be found in (Gustavsen, 1999). By calculating the zeros of $h(s)$, the poles of the original function $f(s)$ can be updated. VF iteratively relocates an initial set of poles to better positions by solving the linear least squares problem in Equation 12 and calculating the zeros of $h(s)$.

The pole identification is followed by a residue identification step. Equation 10 can be solved as an overdetermined linear problem using the relocated poles.

After the first introduction of VF in 1999 (Gustavsen), a relaxed non-triviality constraint is used in the pole identification step of VF to achieve faster convergence and less biasing (Gustavsen, 2006). Additional improvements in the pole identification step were also introduced (Deschrijver, 2008).

Another unique advantage of VF is that the function to be fitted can also be a vector. In this case, all elements in the vector will be fitted using a common pole set. This is very important and useful for the fitting of cross sections of different reactions, as only one set of poles are used for all the reaction types.

4. Generation of the windowed multipole library with point-wise data

This section summarizes the process used in generating a suitable library for OpenMC (Romano, 2013). An overview of the approach is described in Fig. 2~~Fig. 2~~ with a description of the steps below.

(1) Reconstruct the total, elastic scattering, absorption cross sections and any additional reactions available at 0K from ENDF data ~~from ENDF data~~.

In VF, the length of each element in the vector should be the same, however the original point-wise cross sections of different reactions in ~~EDNF~~ ENDF are not using the same energy grid. Therefore,

a union grid is used and the original point-wise cross sections should be interpolated on these grids. For the four nuclides (^{16}O, ^{1}H, ^{10}B, ^{11}B) focused in this paper, only total, elastic scattering, absorption cross sections are considered.

(2) Find out the first threshold energy of each nuclide.

A decision was made to end the fitting process at the first threshold energy of each nuclide. This approach is in line with NJOY, as for most of the nuclides ~~found in the ENDF library where~~ Doppler broadening effects are neglected past the first threshold. Therefore, only the cross sections below the first threshold are needed for poles fitting.

(3) Fit the elastic scattering, absorption cross sections below the first threshold simultaneously, to get the poles and residues.

Below the threshold energy, the total cross section is the sum of the elastic scattering and absorption cross sections. It should be noted that the residues of total cross sections are also equal to the sum of residues of elastic scattering and absorption cross sections. In order to preserve the consistency, the residues of total cross sections were not obtained from VF, but summed from individual reactions.

The elastic scattering and absorption cross sections can be fitted simultaneously with a pre-determined number of poles and an initial guess of poles. VF iteratively updates the poles until the convergence criteria is met. The convergence criterion is set as the relative errors between the fitting results and the point-wise data are smaller than 0.1%.

(4) Sum up the residues of the elastic scattering cross section and the absorption cross section, to get the residues of total cross section.

The poles and the residues of the elastic scattering, absorption and total cross sections are the required input of the windowed multipole procedure.

(5) Set the maximum energy to the first threshold for each nuclide, then choose the inner windowed size and the order of curve fit. Convert the multipole data from VF to windowed multipole library using the windowed multipole procedure (Josey, 2015). Finally, the windowed multipole library was in HDF5 format and can be read directly by OpenMC.

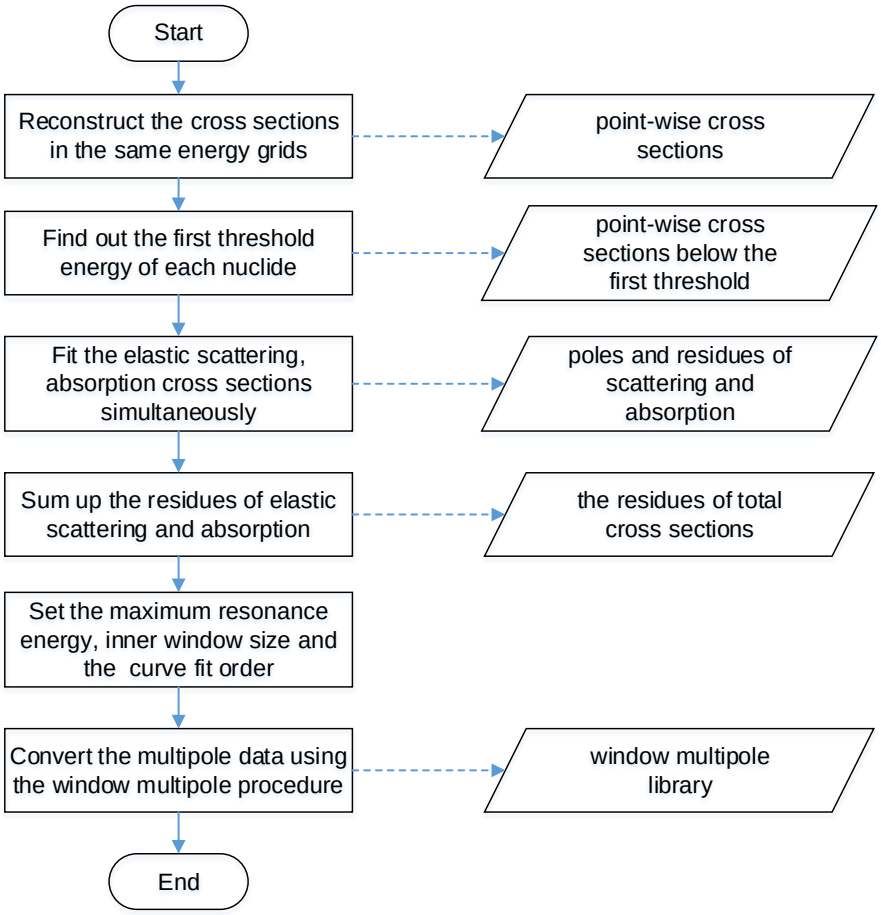

Fig. 2 Procedure of generating windowed multipole library from point-wise data

The number of poles from VF, number of poles in WMP library, average number of poles per window, maximum number of poles per window and number of inner windows are listed in Table 1~~Table 1~~. The number of poles in WMP library are less than the number of poles from VF, because the windowing process replaces certain poles by the low order curve fit.

Table 1 Parameters of windowed multipole library generation

# of poles	# of poles in	Average	Maximum	# of inner

	from VF	WMP library	poles/window	poles/window	windows
^{16}O	203	166	0.682	12	236
^{1}H	32	30	0.014	3	2000
^{10}B	64	50	0.038	2	791
^{11}B	419	202	0.793	58	232

It should be mentioned that in the Vector Fitting procedure in this paper, no efforts were made to avoid overfitting. For example, ^{1}H has no resonances, but the number of poles used in cross sections calculations is 28, which should be zero theoretically.

The overfitting is due to the lack of generalization ability of VF. The objective function in the VF procedure is to get the minimum discrepancies between the fitting results and the original point-wise data at the provided energy points. Therefore, no attention is paid to the linearity between the points just the value at the actual points. Future work will look into simple fixes to reduce overfitting.

5. Results and analysis

The windowed multipole libraries of Oxygen-16, Hydrogen-1, Boron-10 and Boron-11 have been generated using the procedure describe above. The windowed multipole libraries of these four nuclides are added into the original windowed multipole libraries of OpenMC which contains 70 nuclides.

Both the microscopic comparisons and macroscopic comparisons will be performed in this section.

5.1. Microscopic comparisons

In this section, the results of VF for the four nuclides at 0K are compared with the point-wise data. All the comparisons will be performed below the first threshold energy of each nuclide. The first threshold energy of each nuclide is listed in Table 2~~Table 2~~. As ^{1}H has no threshold reaction, the threshold energy is set as the maximum energy of the ENDF data used in OpenMC.

Table 2 First threshold energy of each nuclide

Nuclide	First threshold energy/MeV
^{16}O	2.35532
^{1}H	20.0
^{10}B	0.79071
^{11}B	2.31935

The comparisons of scattering and absorption cross section for these four nuclides are shown in Fig. 3~~Fig. 3~~ to Fig. 10~~Fig. 10,~~ and it can be observed that all of the relative errors (RE) are less than 0.1% at the reference data points. This provides confidence in the accuracy of the generated multipole and the VF algorithm used to get these data.

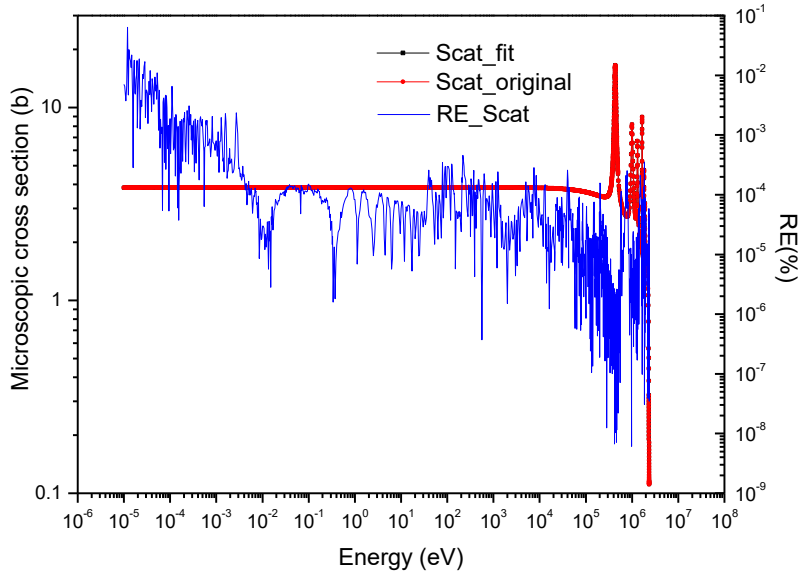

Fig. 3 Comparison of microscopic scattering cross section of ^{16}O (0 K)

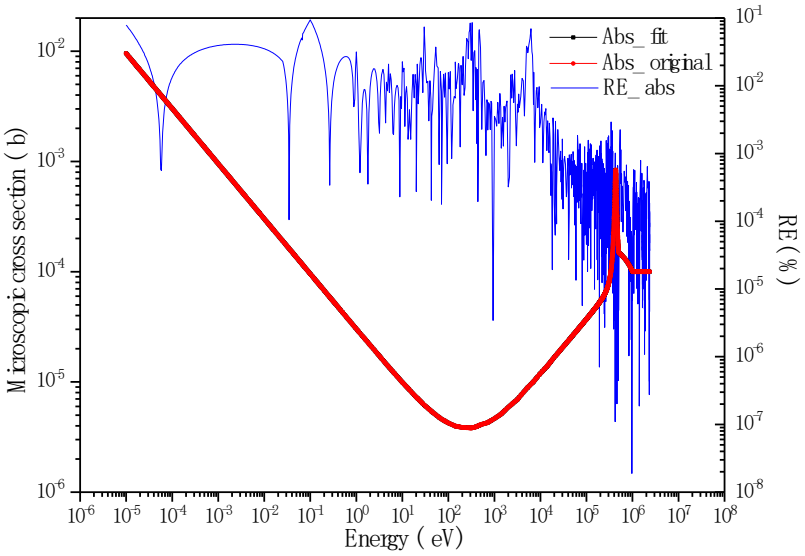

Fig. 4 Comparison of microscopic absorption cross section of ^{16}O (0 K)

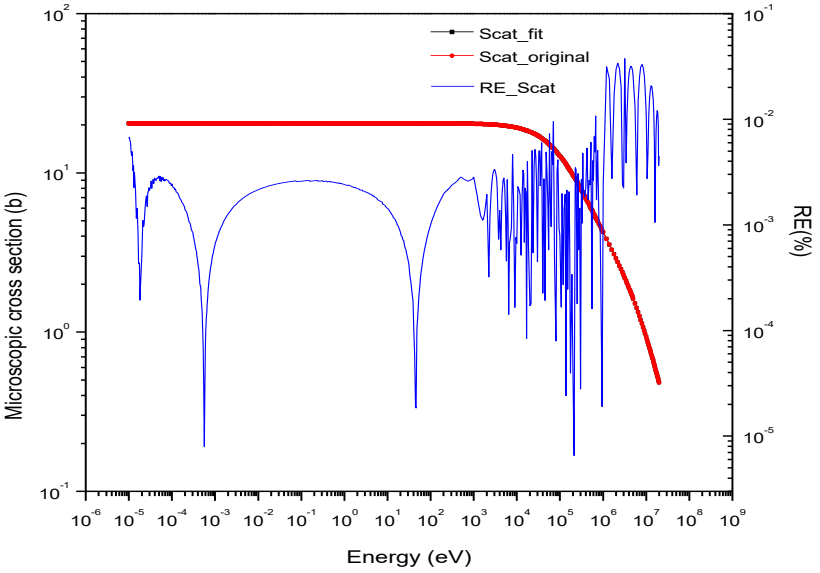

Fig. 5 Comparison of microscopic scattering cross section of ^{1}H (0 K)

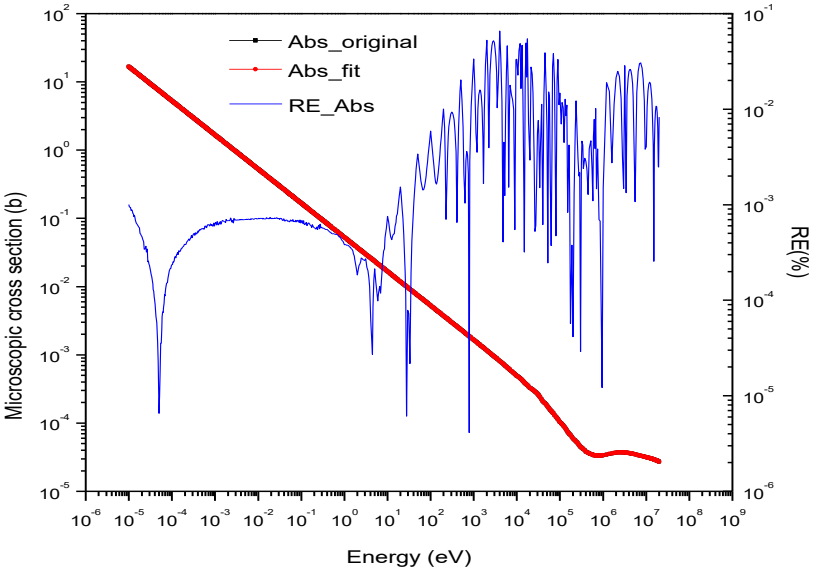

Fig. 6 Comparison of microscopic absorption cross section of ^{1}H (0 K)

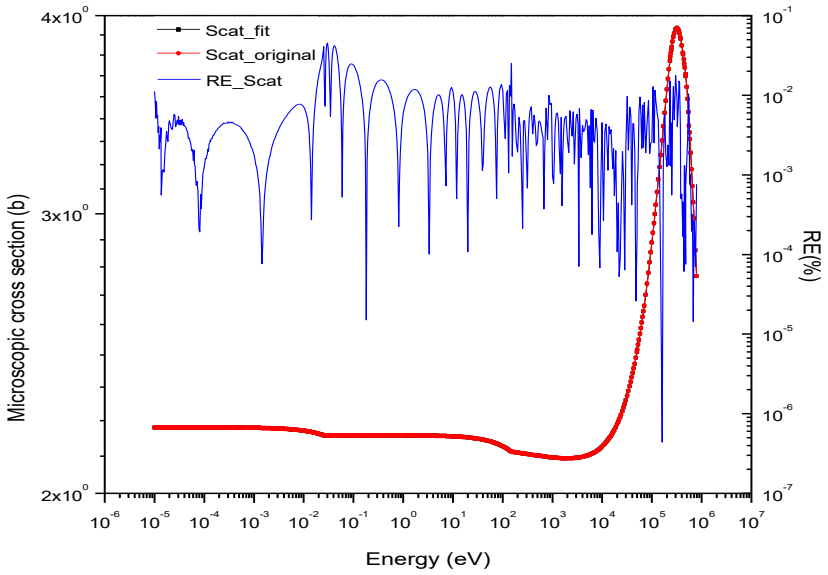

Fig. 7 Comparison of microscopic scattering cross section of ^{10}B (0 K)

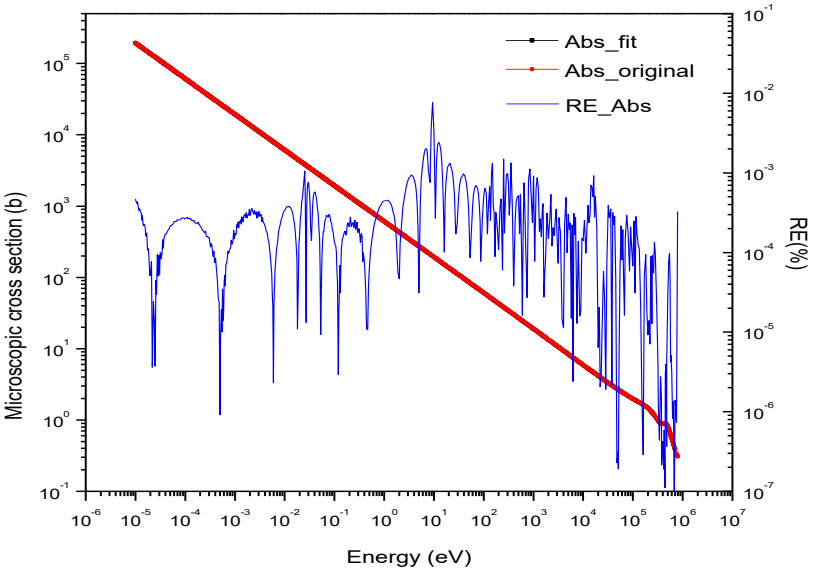

Fig. 8 Comparison of microscopic absorption cross section of ^{10}B (0 K)

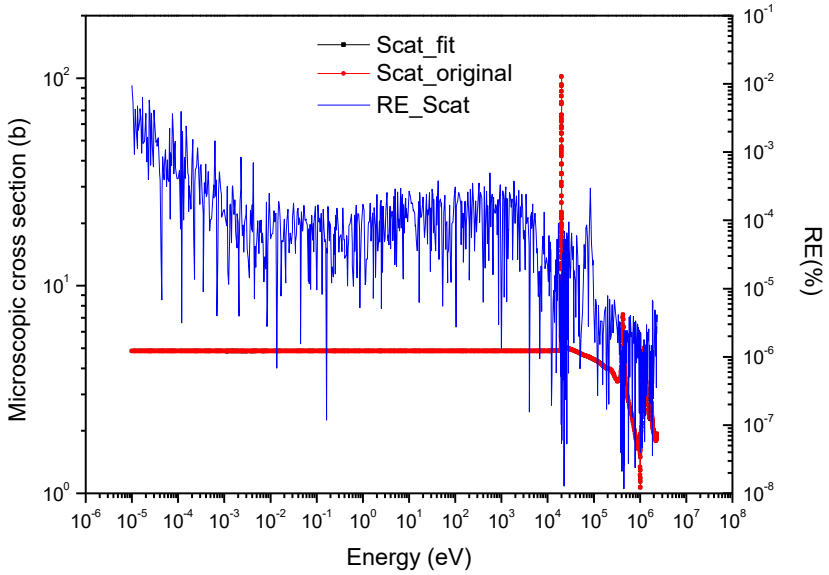

Fig. 9 Comparison of microscopic scattering cross section of ^{11}B (0 K)

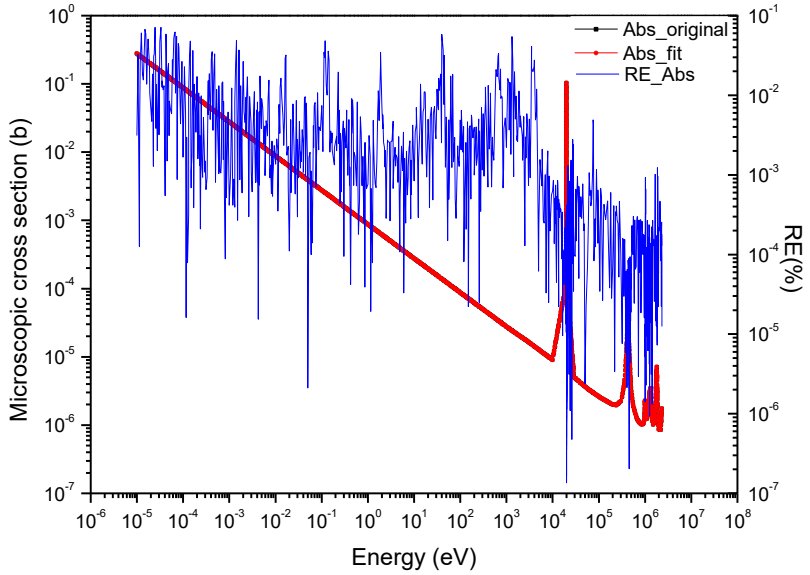

Fig. 10 Comparison of microscopic absorption cross section of ^{11}B (0 K)

Now that the cross sections at 0 K generated by VF have been verified, the multipole data generated by VF can be Doppler broadened to any temperature.

In the second step of microscopic comparisons, the generated windowed multipole data were Doppler broadened to 1500K, and compared with the point-wise data broadened by NJOY which is selected as the reference. It should be noted that in NJOY, the Doppler boarding using the SIGMA1 method will not be performed above a certain energy which is determined as either the upper limit of the resolved resonance range, the first threshold energy of certain reactions or 1 MeV, whichever is lowest. The windowed multipole method on the other hand will only performed Doppler broadening up to the first threshold. This small difference in upper range definition will affect the nuclides whose first threshold energy are above 1 MeV, such as ^{16}O and ^{11}B.

Moreover, during the window generation of windowed multipole method, the outer window is optimized to contain the least number of poles in an effort to minimize the computational cost, while satisfying the accuracy criteria. The accuracy criteria was selected as a relative error below 0.1%, unless the absolute error was below 10^{-5} b, at which point errors are ignored. Therefore, in the comparisons below, both the relative errors and absolute errors are shown.

Fig. 11~~Fig. 11~~ and Fig. 12~~Fig. 12~~ provide the comparisons for ^{1}H at 1500 K where it can be observed that all the relative errors are below 0.1%.

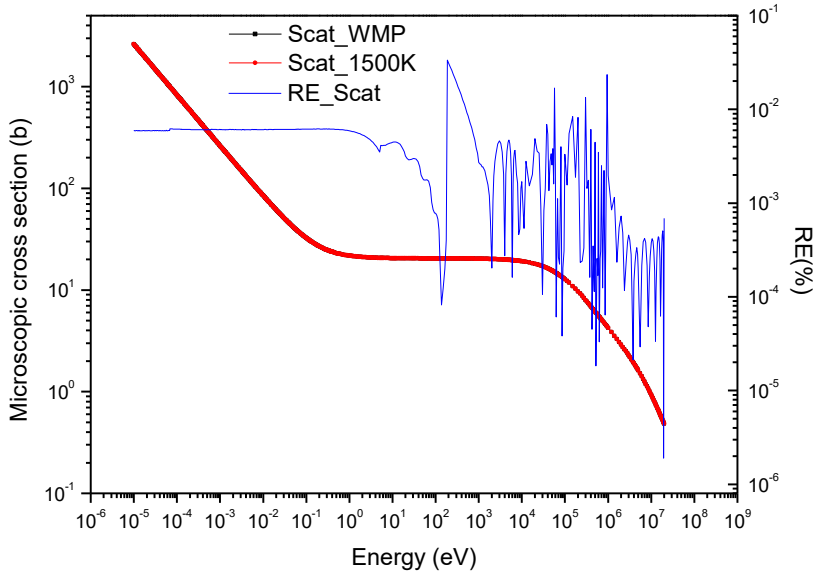

Fig. 11 Comparison of microscopic scattering cross section of ^{1}H (1500 K)

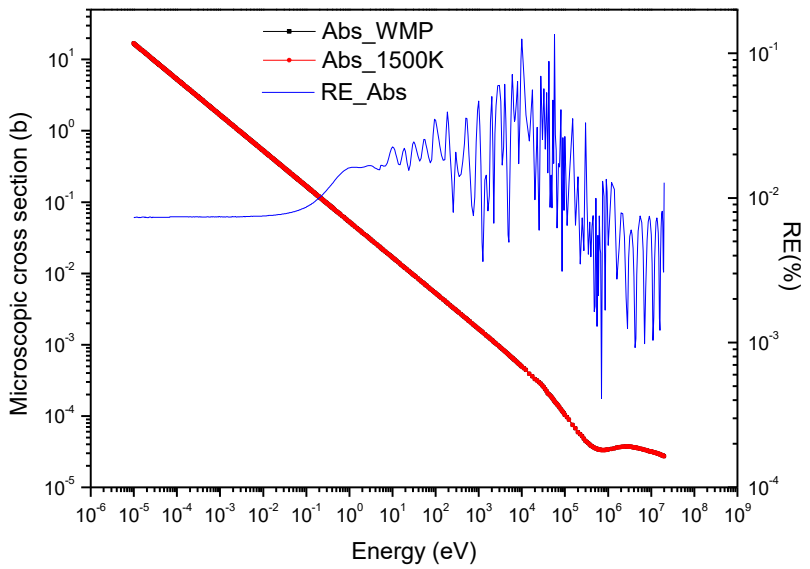

Fig. 12 Comparison of microscopic absorption cross section of ^{1}H (1500 K)

Fig. 13~~Fig. 13~~ and Fig. 14~~Fig. 14~~ are the comparisons for ^{16}O at 1500 K, "Delta" indicates the absolute errors between the two approaches. In Fig. 13~~Fig. 13~~, only a few relative errors of scattering cross section are above 0.1%, among which some are located in energy points above 1 MeV. In Fig. 14~~Fig. 14~~, although the relative errors are large, all of the absolute errors are less than 9×10^{-7} b.

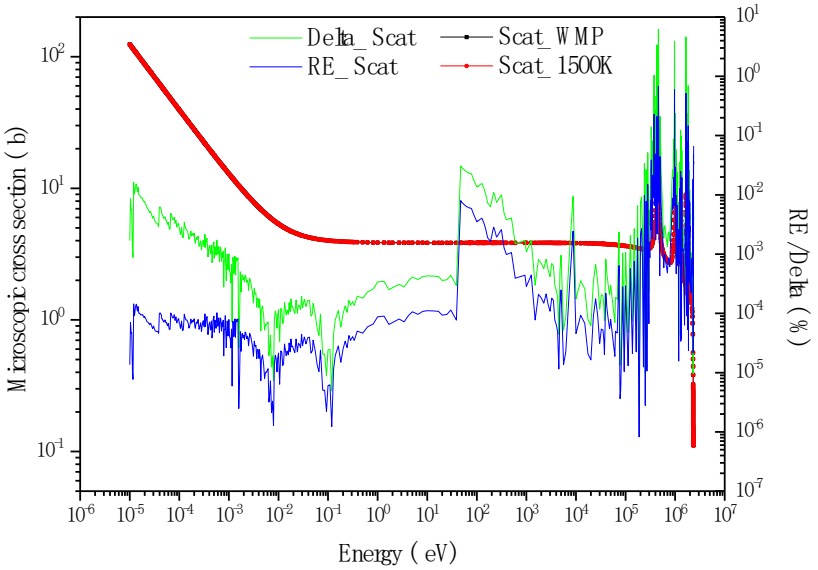

Fig. 13 Comparison of microscopic scattering cross section of ^{16}O (1500 K)

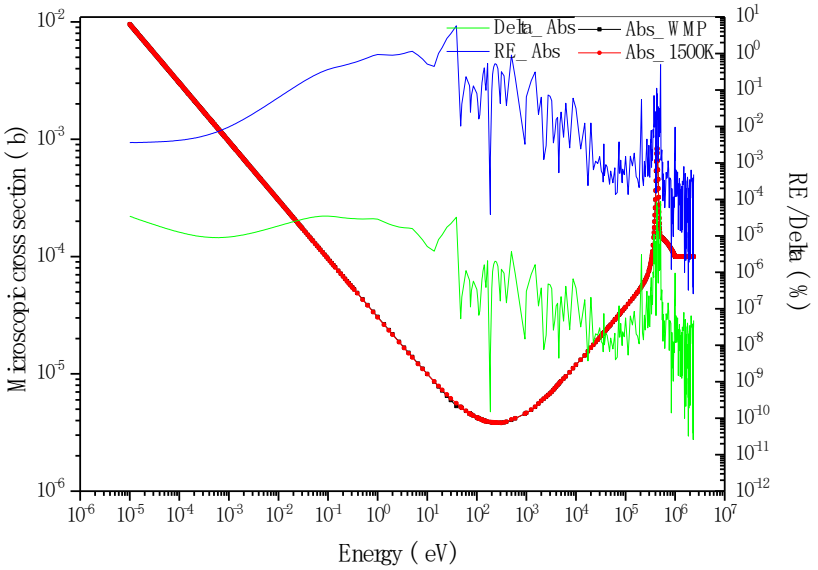

Fig. 14 Comparison of microscopic absorption cross section of ^{16}O (1500 K)

Fig. 15~~Fig. 15~~ and Fig. 16~~Fig. 16~~ are the comparisons for ^{10}B at 1500 K. For both scattering and absorption, all of the relative errors are less than 0.1%.

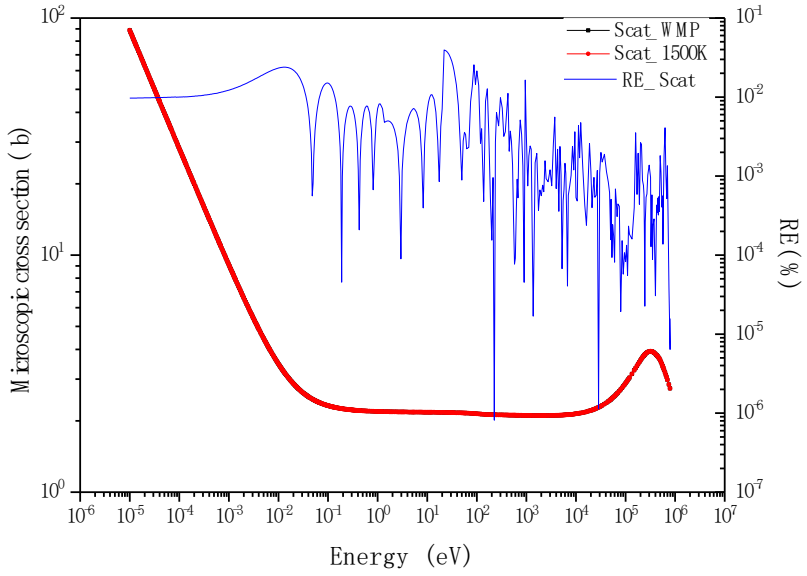

Fig. 15 Comparison of microscopic scattering cross section of ^{10}B (1500 K)

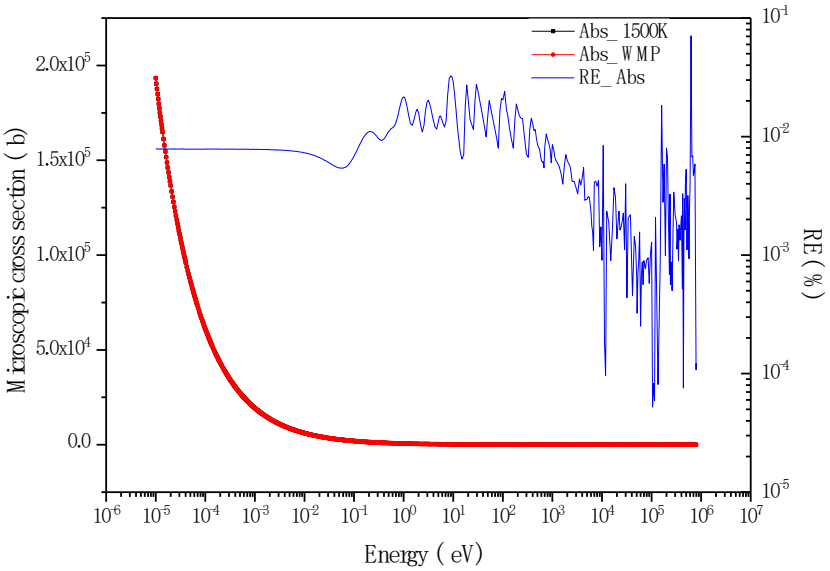

Fig. 16 Comparison of microscopic absorption cross section of ^{10}B (1500 K)

Fig. 17~~Fig. 17~~ and Fig. 18~~Fig. 18~~ are the comparisons for ^{11}B at 1500 K. For the scattering cross section in Fig. 17~~Fig. 17~~, most of the relative errors are below 0.1%. For the absorption cross section in Fig. 18~~Fig. 18~~, the absorption cross section is very small (less than 1 b), thus the relative errors can become quite large. However, the absolute errors are quite small.

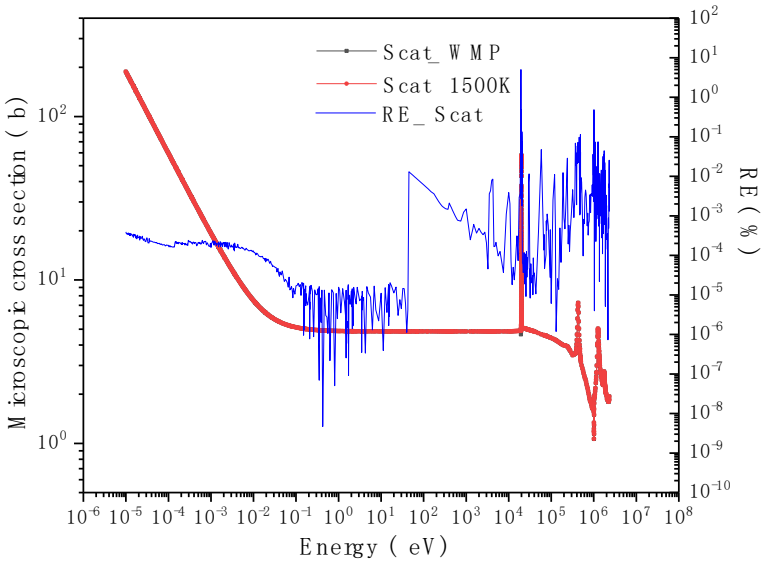

Fig. 17 Comparison of microscopic scattering cross section of ^{11}B (1500 K)

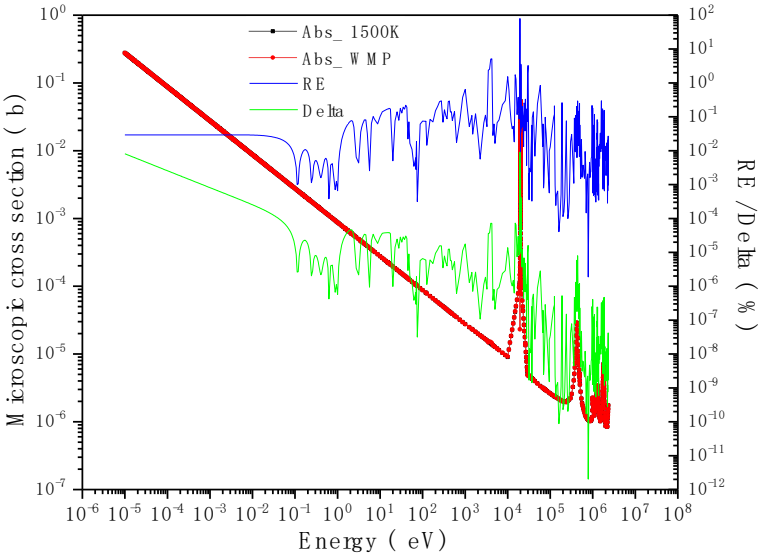

Fig. 18 Comparison of microscopic absorption cross section of ^{11}B (1500 K)

The comparisons in Fig. 11~~Fig. 11~~ to Fig. 18~~Fig. 18~~ demonstrate the ability to vector fit the point-wise and still analytically evaluate the Doppler broadened cross sections.

5.2. Macroscopic comparisons

Three tests were run to analyze the accuracy and efficiency of the windowed multipole method using the generated windowed multipole library for Oxygen-16, Hydrogen-1, Boron-10 and Boron-11. The first case "All_WMP" was performed with the newly generated windowed multipole libraries of the four nuclides. The second case "WMP +ACE" was performed with the originally existing windowed multipole libraries of the 70 nuclides, but with the four nuclides in ACE format. The third case "All_ACE" was performed without the windowed multipole libraries, but with the traditional point-wise libraries in ACE format.

A typical fuel pin case in pressurized water reactors was used, which was taken from the BEAVRS benchmark (Horelik, 2013). The fuel pin has cladding, an air gap and fuel of 1.6% enrichment, surrounded by borated water, as shown in Fig. 19~~Fig. 19~~. The nuclide densities of materials of the fuel pin model are listed from Table 3~~Table 3~~ to Table 6~~Table 6~~. The windowed multipole data of Oxygen-16 was applied to

the moderator, cladding and fuel, while that of Hydrogen-1, Boron-10 and Boron-11 were applied to the moderator.

As the ACE libraries of 300K were used, the on-the-fly Doppler broadening was performed by setting the temperature of all the material to 300K. The neutron transport calculations were performed by OpenMC, and the 238-group flux and reaction rates were tallied in the fuel and moderator. The calculation parameters are listed in Table 7~~Table 7~~.

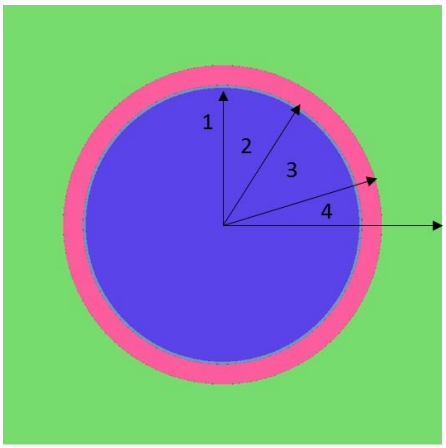

Arrow	Radius (cm)	Material
1	0.39218	Fuel
2	0.40005	Helium
3	0.45720	Zircaloy
4	0.62992	Coolant

Fig. 19 Fuel pin model

Table 3 Nuclide densities of fuel 1.6% enriched

Density (g/cc)	10.31341
Isotope	Number Density (atom/b-cm)
^{234}U	3.0131×10^{-6}
^{235}U	3.7503×10^{-4}
^{238}U	2.2625×10^{-2}
^{16}O	4.5895×10^{-2}
^{17}O	1.7482×10^{-5}
^{18}O	9.4313×10^{-5}

Table 4 Nuclide densities of Helium

Density (g/cc)	0.001598
Isotope	Number Density (atom/b-cm)
^{4}He	2.4044×10^{-4}

Table 5 Nuclide densities of Zircaloy 4

Density (g/cc)	6.55
Isotope	Number Density (atom/b-cm)

^{16}O	3.0743×10^{-4}
^{17}O	1.1711×10^{-7}
^{18}O	6.3176×10^{-7}
^{50}Cr	3.2962×10^{-6}
^{52}Cr	6.3564×10^{-5}
^{53}Cr	7.2076×10^{-6}
^{54}Cr	1.7941×10^{-6}
^{54}Fe	8.6699×10^{-6}
^{56}Fe	1.3610×10^{-4}
^{57}Fe	3.1431×10^{-6}
^{58}Fe	4.1829×10^{-7}
^{90}Zr	2.1827×10^{-2}
^{91}Zr	4.7600×10^{-3}
^{92}Zr	7.2758×10^{-3}
^{94}Zr	7.3734×10^{-3}
^{96}Zr	1.1879×10^{-3}
^{112}Sn	4.6735×10^{-6}
^{114}Sn	3.1799×10^{-6}
^{115}Sn	1.6381×10^{-6}
^{116}Sn	7.0055×10^{-5}
^{117}Sn	3.7003×10^{-5}
^{118}Sn	1.1669×10^{-4}
^{119}Sn	4.1387×10^{-5}
^{120}Sn	1.5697×10^{-4}
^{122}Sn	2.2308×10^{-5}
^{124}Sn	2.7897×10^{-5}

Table 6 Nuclide densities of coolant water

Density (g/cc)	0.740582
Isotope	Number Density (atom/b-cm)
^{10}B	8.0042×10^{-6}
^{11}B	3.2218×10^{-5}
^{1}H	4.9457×10^{-2}
^{2}H	7.4196×10^{-6}
^{16}O	2.4672×10^{-2}
^{17}O	9.3982×10^{-6}
^{18}O	5.0701×10^{-5}

Table 7 Calculation conditions

Parameter	Value
Inactive cycles	30
Active cycles	120
Neutrons per cycle	10^6
Number of processors	24

The k_{inf} of the three cases are compared in Table 8~~Table 8~~, in which the "WMP +ACE" case was selected as reference. The standard deviation is noted as "SD". It can be found that the differences of k_{inf} are all within one standard deviation.

Table 8 k_{inf} of three cases

	# of nuclides with WMP libraries	k_{inf}	SD	Δk
All_WMP	74	1.029787	8.17×10^{-5}	4.12×10^{-5}
WMP +ACE	70	1.029746	7.32×10^{-5}	0
All_ACE	0	1.029686	8.55×10^{-5}	-5.98×10^{-5}

Moreover, the flux and reactions rates were also compared. In order to evaluate the impact of the 4 nuclides that were vector fitted, the "WMP +ACE" case was selected as reference. The fluxes in fuel are compared between "WMP +ACE" and "All_WMP" in Fig. 20~~Fig. 20~~. It can found that most of the relative errors (RE) are less than 1%, while the large errors appear at energies with very low flux.

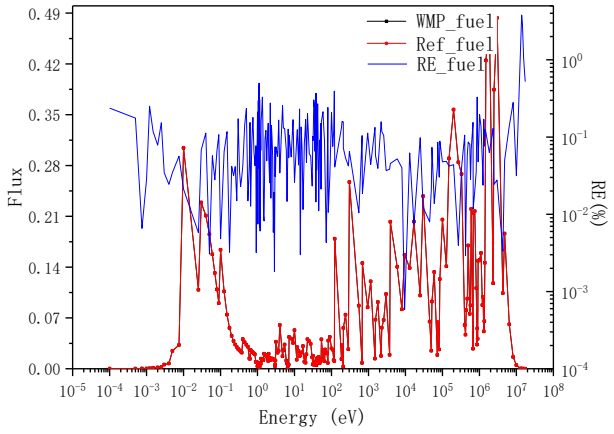

Fig. 20 Flux and RE in fuel

The relative errors (RE) and three times of the relative stand deviations (3σ) are also compared in

Fig. 21~~Fig. 21~~. It can be found that almost all of the REs are within the 3σ criteria, showing good agreements between WMP and ACE libraries for the four nuclides.

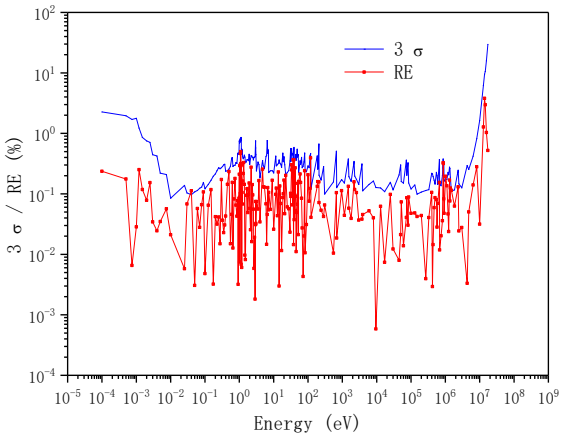

Fig. 21 RE and SD for flux in fuel

The fluxes in the moderator are also compared in Fig. 22~~Fig. 22~~, in which most of the relative errors are less than 1%. In Fig. 23~~Fig. 23~~, almost all of the RE are within the 3σ criteria, showing the accuracy of WMP libraries for the four nuclides.

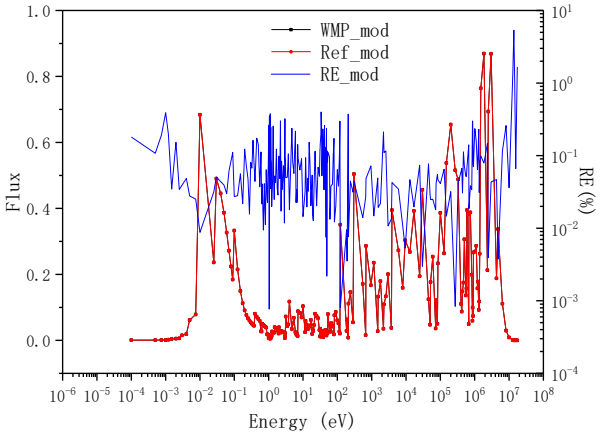

Fig. 22 Flux in moderator

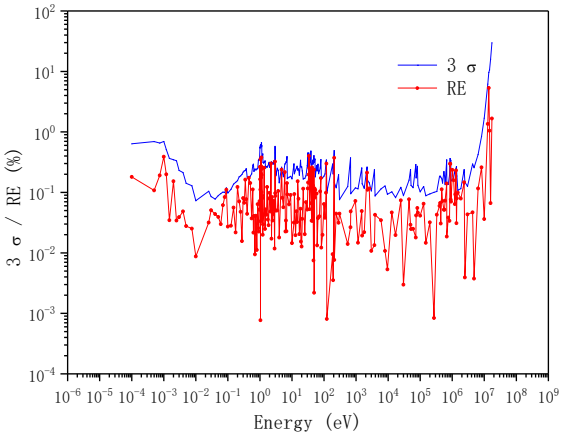

Fig. 23 RE and SD for flux in moderator

The scattering rate of ^{1}H in moderator, absorption rate of ^{10}B in moderator, scattering rate of ^{10}B in moderator, total reaction rate of ^{16}O in fuel and moderator are shown in Fig. 24~~Fig. 24~~ to Fig. 28~~Fig. 28~~ respectively. It can be found that most of the relative errors (RE) are less than 1%, while the large errors appear in the energies where the reactions rates are small.

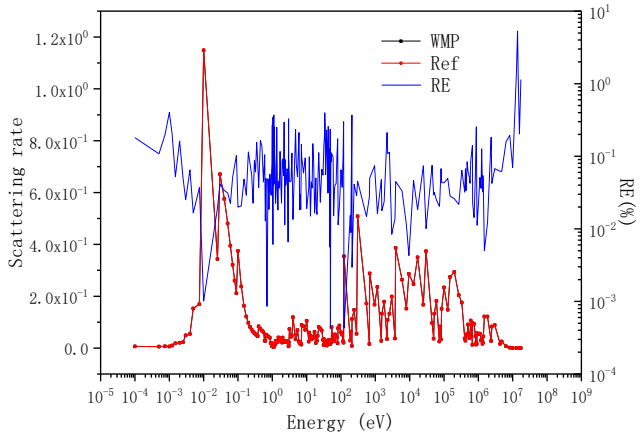

Fig. 24 Scattering rate of ^{1}H in moderator

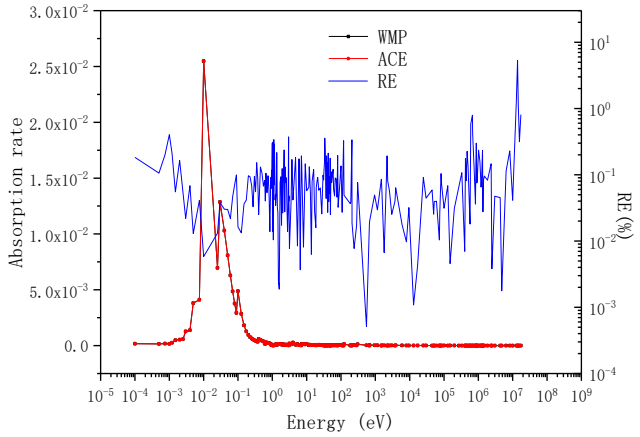

Fig. 25 Absorption rate of ^{10}B in moderator

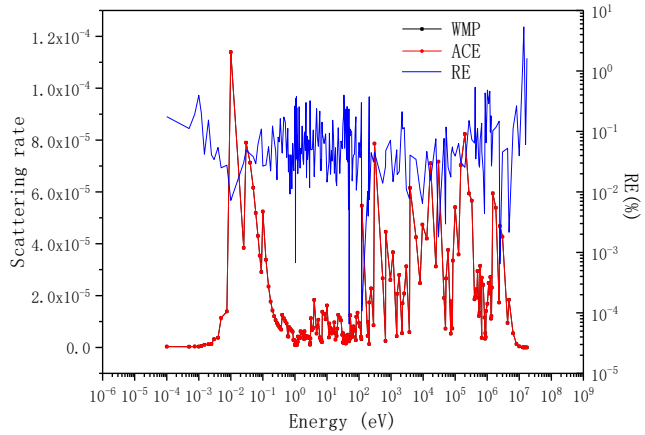

Fig. 26 Scattering rate of ^{11}B in moderator

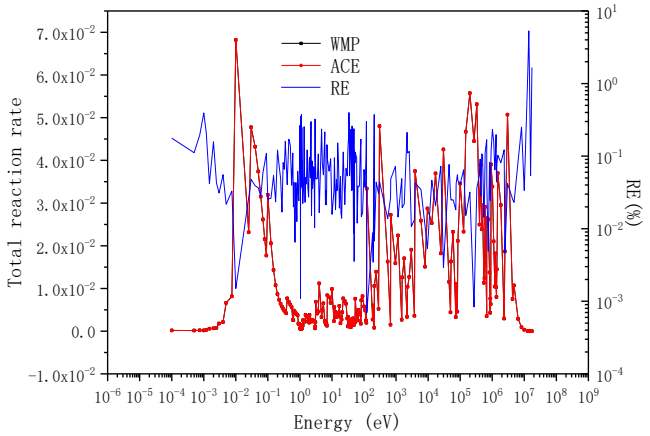

Fig. 27 Total reaction rate of ^{16}O in moderator

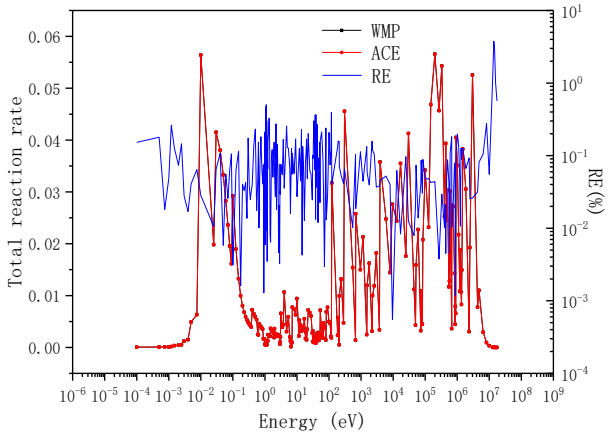

Fig. 28 Total reaction rate of ^{16}O in fuel

The calculation time of three cases is listed in Table 9~~Table 9~~. The single temperature "All_ACE" is the fastest and selected as reference for comparison. The "WMP +ACE" with 70 nuclides has WMP libraries is 23% slower, while the "All_WMP" with 74 nuclides has WMP libraries is 28% slower, compared to the case without WMP libraries. It should be noted that the runtime increase is for a pin cell with a very simple geometry at 300K. For an assembly or full core problem at operating temperatures, the increase of the overall runtime would be less than 28% with the flexibility of simulating different temperatures in every cell.

Table 9 Calculation time of three cases

	Total calculation time/Mins	Ratio
All_WMP	97.86	1.28
WMP +ACE	94.26	1.23
All_ACE	76.33	1.0

6. Conclusions

On-the-fly Doppler broadening is one of the key features needed to enable high fidelity multiphysics simulations using Monte Carlo methods. The windowed multipole representation is one of the most promising method for on-the-fly Doppler broadening due to its limited memory footprint and efficiency.

In this paper, a new approach for fitting the nuclear point-wise cross sections in ENDF data was proposed using the Vector Fitting technique which provides a practical way to convert the point-wise cross sections data to the windowed multipole format. This procedure can be effectively applied to the nuclides for which no resonance parameters are provided in the ENDF/B-VII.1 evaluation.

Four important nuclides needed in reactor applications: Oxygen-16, Hydrogen-1, Boron-10 and Boron-11, were used to demonstrate the feasibility and accuracy of the new approach. Using the Vector Fitting technique, a windowed multipole library was generated for these four nuclides.

These new libraries were tested by both direct comparison of the microscopic cross sections at 0K and 1500K, and by integral comparisons using a typical PWR pin cell from the BEAVRS benchmark. For the microscopic comparisons, all of the relative errors between the fitting results and the point-wise cross sections are below 0.1% at 0 K. The microscopic cross sections at 1500 K agree well with the reference solutions obtained using the SIGMA1 method with a few values exceeding the 0.1% value but only for very low cross section values (below 10^{-5} b). For the macroscopic comparisons, the differences of k_{inf} are within one standard deviation. Most of the relative errors (RE) of flux and reactions rates are less than 1%, while the large errors appear in the energies where the low flux and reaction rates are very low.

The run times of windowed multipole representation are 28% slower when using 74 nuclides in WMP format compared to a single temperature ACE library.

For the future work, two goals will be focused on. First is the regularization process to improve the generalization ability of Vector Fitting, so as to conquer the problem of overfitting. The second goal is to generate a full WMP library including all the nuclides, using the generalized Vector Fitting technique.

Acknowledgments

This research was supported in part by the Consortium for Advanced Simulation of Light Water Reactors (CASL), an Energy Innovation Hub for Modeling and Simulation of Nuclear Reactors under U.S. Department of Energy Contract No. DE-AC05-00OR22725. The first author is partially supported by Tsinghua Scholarship for Overseas Graduate Studies. The second author is partially supported by China Scholarship Council. The third author is partially supported under a Department of Energy Nuclear Energy University Programs Graduate Fellowship.

Reference

Becker B. et al., 2009. An Alternative Stochastic Doppler Broadening Algorithm. Proc. M&C 2009, Saratoga Springs, New York, May 3–7, 2009.

Cullen, D.E., Weisbin, C.R., 1976. Exact Doppler broadening of tabulated cross sections. Nucl. Sci. Eng. 60 (3), 199–229. http://dx.doi.org/10.13182/NSE76-1.Deschrijver, D., Mrozowski, M.,

Dhaene, T., & De Zutter, D., 2008. Macromodeling of multiport systems using a fast implementation of the vector fitting method. IEEE Microwave & Wireless Components Letters, 18(6), 383-385.
Forget, B., Xu, S., and Smith, K., 2014. Direct Doppler broadening in Monte Carlo simulations using the multipole representation, Ann. Nucl. Energy 64, 78–85.
Gustavsen, B., & Semlyen, A. 1999. Rational approximation of frequency domain responses by vector fitting. IEEE Transactions on Power Delivery, 14(3), 1052-1061.
Gustavsen, B. 2006. Improving the pole relocating properties of vector fitting. IEEE Transactions on Power Delivery, 21(3), 1587-1592.
Herman, B.R., Forget, B., Smith, K., 2014. Progress toward Monte Carlo-thermal hydraulic coupling using low-order nonlinear diffusion acceleration methods, Ann. Nucl. Energy 84, 75–86, http://dx.doi.org/10.1016/j.anucene.2014.10.029.
Horelik, N., Herman, B., Forget, B., Smith, K., MIT BEAVRS: Benchmark for evaluation and validation of reactor simulations, in: International Conference on Mathematics and Computational Methods Applied to Nuclear Science and Engineering, Sun Valley, ID, 2013.
Hwang, R.N., 1987. A rigorous pole representation of multilevel cross sections and its practical applications, Nucl. Sci. Eng. 96, 192–209.
Josey, C., Forget, B., Smith, K., Efficiency and accuracy evaluation of the windowed multipole direct Dopplerbroadening method, in: Proceedings of PHYSOR 2014, 2014.
Josey, C., Ducru, P., Forget, B., & Smith, K., 2016. Windowed multipole for cross section doppler broadening. Journal of Computational Physics, 307, 715-727.
Josey, C., Forget, B. & Smith, K., 2015. Windowed multipole sensitivity to target accuracy of the optimization procedure, Journal of Nuclear Science and Technology, 52:7-8, 987-992
Romano, P.K., Forget, B., 2013. The OpenMC Monte Carlo particle transport code. Annals of Nuclear Energy 51, 274–281.
Romano, P. K., & Trumbull, T. H., 2015. Comparison of algorithms for doppler broadening pointwise tabulated cross sections. Ann. Nucl. Energy, 75, 358-364.
Solbrig, A.W., 1961. Doppler broadening of low-energy resonances. Nucl. Sci. Eng. 10, 167–168.
Viitanen, T., Leppänen, J., 2012. Explicit Treatment of Thermal Motion in Continous-Energy Monte Carlo Tracking Routines, Nucl. Sci. Eng. 171, 165.
Wang, K., et al., 2017. Analysis of BEAVRS two-cycle benchmark using RMC based on full core detailed model. Progress in Nuclear Energy 98, 301-312.
Yesilyurt, G., Martin, W.R., Brown, F., 2012. On-the-Fly Doppler Broadening for Monte Carlo Codes, Nucl. Sci. Eng. 171, 239.